

PAPER • OPEN ACCESS

## Facile modification of freestanding silicon nitride microcantilever beams by dry film photoresist lithography

To cite this article: Madeleine Nilsen *et al* 2019 *J. Micromech. Microeng.* **29** 025014

View the [article online](#) for updates and enhancements.

You may also like

- [Microfabrication of bulk PZT transducers by dry film photolithography and micro powder blasting](#)  
I Misri, P Hareesh, S Yang et al.
- [Print-to-pattern dry film photoresist lithography](#)  
Shaun P Garland, Terrence M Murphy and Tingrui Pan
- [Microstructuring characteristics of a chemically amplified photoresist synthesized for ultra-thick UV-LIGA applications](#)  
Chii-Rong Yang, Gen-Wen Hsieh, Yu-Sheng Hsieh et al.

# Facile modification of freestanding silicon nitride microcantilever beams by dry film photoresist lithography

Madeleine Nilsen<sup>1</sup> , Fabian Port<sup>2</sup>, Michael Roos<sup>1</sup>,  
Kay-Eberhard Gottschalk<sup>2</sup> and Steffen Strehle<sup>1</sup>

<sup>1</sup> Ulm University, Institute of Electron Devices and Circuits, Albert-Einstein-Allee 45, 89081 Ulm, Germany

<sup>2</sup> Ulm University, Institute of Experimental Physics, Albert-Einstein-Allee 11, 89081 Ulm, Germany

E-mail: [steffen.strehle@uni-ulm.de](mailto:steffen.strehle@uni-ulm.de)

Received 17 October 2018, revised 6 December 2018

Accepted for publication 11 December 2018

Published 14 January 2019



## Abstract

A photolithographic technique based on dry film photoresists for facile and low-cost patterning of microcantilever beams is presented. Dry film photoresists enable instantly homogenous photoresist coatings on flexible and 3D patterned substrate surfaces, represented here by microcantilever beams, which is otherwise challenging if conventional spin-coating of photoresist is utilized. Compared to alternative microtechnologies, such as focused ion beam milling or resist spray coating, our strategy is far less elaborate, fully compatible with routine additive and subtractive microfabrication processes and can be readily scaled. We show specifically microcantilever shape modification by  $\text{CF}_4$  reactive ion etching, localized metal deposition in combination with conventional lift-off procedures as well as a utilization of patterned dry film photoresists as permanent microstructural elements. These microstructural elements are in particular flat-ended cylindrical dry resist micropillars created at the freestanding end of the cantilever beam that can be employed as scanning probes. The resist pillars enabled imaging of a 3T3 mouse fibroblast cell culture surface to determine their elastic force constants. Alongside UV-exposure by a conventional mask aligner, we also demonstrate dry film photoresist exposure by contact-free laser lithography eliminating possible substrate damage by photomask contact.

Keywords: microcantilevers, negative resist, AFM, cell elasticity, dry film photoresist, lithography

 Supplementary material for this article is available [online](#)

(Some figures may appear in colour only in the online journal)

## 1. Introduction

Microcantilever based sensors have seen a surge in popularity going along with the invention of atomic force microscopy (AFM) and consequent availability of microfabricated cantilever beams [1]. By microcantilever beam we imply here a suspended microstructure having a much smaller thickness and width compared to its length, which typically ranges between 100 to 300  $\mu\text{m}$ . Perhaps the most well-known cantilever sensor application is topography mapping in AFM,

where local interaction forces between the sample surface and a sharp tip situated on the cantilever's free end are exploited to reconstruct the nanoscale surface profile. Cantilever tips are furthermore prominent tools to measure micro- and nano-mechanical properties comprising cell elasticity and molecular binding forces in so-called force spectroscopy. For the detection of chemical or biochemical species, tipless cantilevers are more common and do not involve AFM raster scanning of a surface. One side of the cantilever is here typically homogeneously coated with a marker layer able to specifically bind



certain molecular species. This results either in a shift of the cantilever resonance frequency, or in a mass and medium density induced change of the beam deflection [1]. Contrary to a homogenous cantilever coating are specifically patterned coatings to realize for instance complex sensor designs, the implementation of electrodes or an integration of multiple functional materials on the freestanding microcantilever [2–9]. In principle, well-established photolithography is a relatively efficient method to realize material micropatterning. Nevertheless, conventional direct spin-coating of liquid photoresists onto freestanding, flexible, and 3D-structured cantilevers is rather challenging mainly due to so-called edge-bead effects [10, 11]. These edge-bead effects result in an inhomogeneous resist layer thickness, which typically yields dissatisfying results for resist exposure and development. Fabrication of desired microstructures on the prospective freestanding microcantilever beam is therefore, realized in most cases prior to cantilever fabrication, meaning prior to its bulk substrate release. Although this strategy appears straightforward, the overall material compatibility must be matched within the entire fabrication process, which means for instance that required dry and wet etching steps for the cantilever release shall not damage the previously patterned functional materials.

In order to tackle these challenges, some strategies were already presented elsewhere. Those methods comprise focused ion beam (FIB) milling [12], ice resist [13] and resist spray coatings of either photo- or electron beam sensitive resists [14, 15]. Despite the fact that nanometer resolution can be reached by both, electron beam lithography and FIB milling, their overall technological availability, the overall costs and the significant time-consumption limit their usability with emphasis to device yield and batch fabrication. What has yet to be demonstrated is therefore a simple and cost-effective strategy enabling photolithography directly on non-planar, freestanding, flexible surfaces such as microcantilever beams, which would widen and ease the microfabrication of novel electro-mechanical microsystems significantly. Based on dry film photoresists, which can be directly attached to a substrate by plain thermal lamination, this challenge can be addressed.

The general principle of the strategy presented here is in its core similar to a method presented by Chang *et al* [16] who fabricated 200 nm thick solid electron-sensitive PMMA dry film photoresist sheets by spin-coating. These PMMA films were directly transferred onto various non-planar substrate surfaces such as edges, silicon nitride bridges and deposited gold wires, followed by conventional electron beam lithography, metal deposition and resist lift-off. Instead, we take advantage of optical dry film photoresist lithography (DFPL) to pattern freestanding microcantilever beams using negative tone dry epoxy photoresist films. The dry film photoresists exhibit already a superior homogeneity in film thickness and are commercially available in contrast to electron sensitive dry film photoresist. The dry film photoresists implemented here are compatible with conventional UV-source mask aligners and direct writing contact-free UV-laser lithography. They enable therefore rapid, affordable, reproducible and reliable microfabrication at a large scale in comparison

to the aforementioned competing methods. Specifically, we show DFPL applicability for the customization of in-house fabricated tipless silicon nitride cantilever beams, as well as commercial silicon nitride AFM cantilevers with pyramidal scanning tips. The in-house fabricated probes are also compatible with conventional AFM. In order to modify the freestanding microcantilever beams both, subtractive or additive microfabrication processes are demonstrated. In this regard, we show for instance the implementation of the dry film photoresists as a protective mask for  $\text{CF}_4$  plasma reactive ion etching (RIE), allowing precise etching of cantilevers, as well as their use in combination with metal deposition and conventional wet lift-off to create customized metal patterns. Finally, the efficient creation of flat-ended cylindrical dry photoresist pillar tips on in-house fabricated microcantilevers is demonstrated as well as their successful employment in cell elasticity measurements of 3T3 mouse fibroblasts.

## 2. Material and methods

### 2.1. In-house fabrication of AFM compatible tipless silicon nitride microcantilever beams

The in-house fabrication of tipless silicon nitride microcantilever beams on  $1.5 \times 3.5$  mm AFM-sized probe bodies is illustrated in detail in figure 1. As initial substrate, a 4 inch single-crystalline  $380 \mu\text{m}$  thick (100)-Si wafer with  $1 \mu\text{m}$  double-side coating of low-stress silicon nitride deposited by low-pressure chemical vapor deposition (purchased from MicroChemicals GmbH) was diced into pieces of up to  $30 \times 30 \text{mm}^2$ . Each chip is able to carry a maximum of 28 cantilever probes. Our strategy comprises the direct fabrication of microcantilevers by a localized dry etching of silicon nitride membranes created by wet-chemical KOH etching of the silicon substrate starting from the backside of the sample. Initial probe patterning was realized by conventional photolithography using the photoresist AZ 5214E, spin-coated at 4000 rpm for 60 s on both sides of the wafer, and subsequently baked for 90 s at  $110 \text{ }^\circ\text{C}$  under ambient conditions. The sample backside was brought into contact with an appropriate quartz photomask and exposed 30 s using a 4 inch mask aligner operating at 405 nm wavelength (Süss MJB4 mask aligner,  $4 \text{ mW cm}^{-2}$ ). After exposure, immersion development was performed using the AZ 726 MIF developer. The silicon nitride film present on the developed side was then locally removed in areas that were not protected by the photoresist utilizing a 20 min RIE (Plasma Therm, Model 2484) at a flow of 50 sccm  $\text{CF}_4$  at  $5.33 \cdot 10^{-2}$  mbar working pressure (600 W power, figure 1(b)). The photoresist was finally removed in acetone. The remaining patterned silicon nitride films act as a hard mask in the following chemical wet-etch of silicon performed at  $80 \text{ }^\circ\text{C}$  for 8 h in 20 wt % KOH dissolved in a 2:1 solution of water and isopropanol. After silicon etching from the backside through the entire wafer, the  $1 \mu\text{m}$  silicon nitride top-layer persisted locally as silicon nitride membranes (figures 1(c) and (d)).

These local membranes resemble the substrate for the microcantilever beam patterning within a subsequent etching

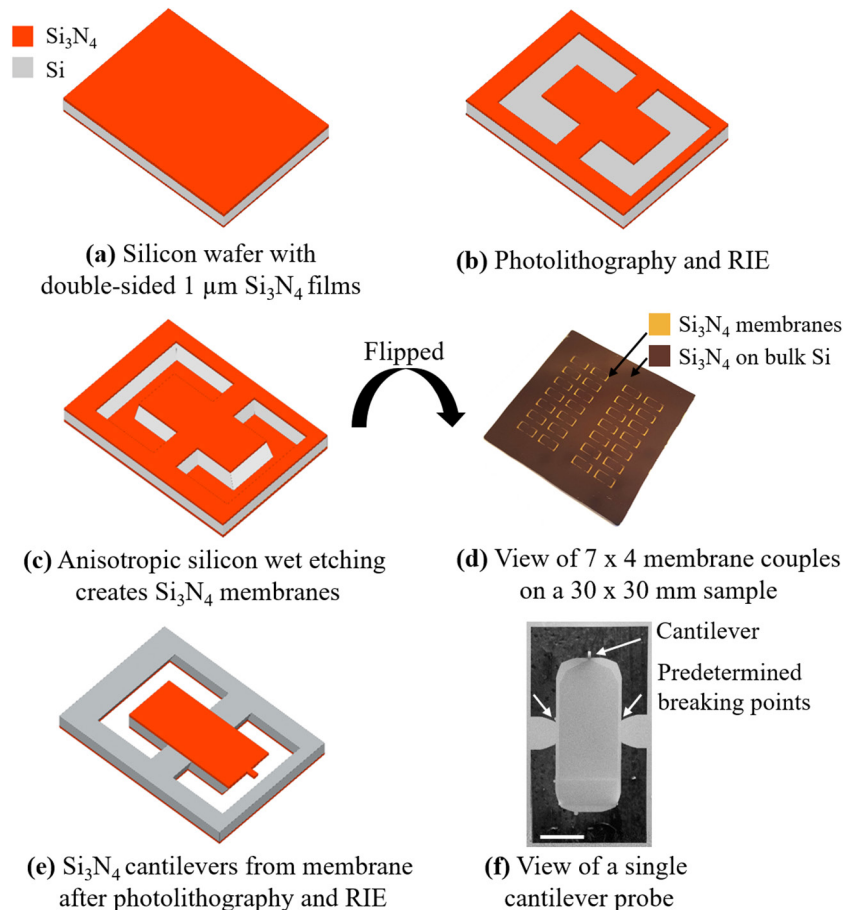


**Figure 1.** Fabrication schematic of the in-house microfabrication process of tipless silicon nitride cantilever probes. (a) Starting material is a  $380\ \mu\text{m}$  thick (100)-Si wafer, with a  $1\ \mu\text{m}$  low stress silicon nitride coating (LPCVD- $\text{Si}_3\text{N}_4$ ) on both sides. (b) By conventional photolithography using spin-coating of a positive liquid photoresist, UV-exposure using mask aligner and resist development, silicon nitride is partially etched by  $\text{CF}_4$  plasma RIE revealing the silicon substrate underneath. (c) The remnant silicon nitride subsequently functions as a hard mask when the sample is immersed in 20 wt % KOH solution where silicon undergoes anisotropic chemical wet-etching. (d) Silicon nitride membranes are clearly visible after completion of the KOH etching when flipping the sample to its frontside. Shown are all the  $4 \times 7$  prospective cantilever probes and the intact silicon nitride membranes. (e) Cantilevers are fabricated from these membranes employing conventional photolithography and a liquid photoresist on the planar substrate surface. Resist development is followed by RIE of the silicon nitride membranes with  $\text{CF}_4$  plasma. Resist removal takes place in warm NEP, finally producing clean silicon nitride cantilevers on an AFM sized probe body as seen in (f), with  $1\ \mu\text{m}$  scale bar. Prior to the cantilever modification, the probes are mechanically released from the main substrate by means of the predetermined breaking points.

step. Here, the photoresist AZ 5214E was again spin-coated on the planar membrane substrate surface, exposed with the cantilever design, developed and dry-etched by RIE in a  $\text{CF}_4$ -plasma following the aforementioned manner. This process yields finally tipless microcantilever beams of approximately  $1\ \mu\text{m}$  in thickness (figures 1(e) and (f)). A complete resist removal necessitated immersion in  $100\ ^\circ\text{C}$  N-Ethyl-2-pyrrolidone (NEP), followed by oxygen plasma etching at 9 sccm flow of  $\text{O}_2$  at  $1.33 \cdot 10^{-1}$  mbar pressure (95 W power) for 20 min (Plasmalab,  $\mu$ -etch). The length of the microcantilevers was systematically varied between  $150\ \mu\text{m}$  and  $200\ \mu\text{m}$ , and the width between  $60\ \mu\text{m}$  and  $70\ \mu\text{m}$ , as representative dimensions of commercial AFM cantilever beams. After cantilever modification by DFPL as described in the following sections, gentle mechanical pressing onto the body of the cantilever probes released them from the bulk substrate by fracture at predetermined breaking points (figure 1(f)).

## 2.2. DFPL on in-house fabricated cantilevers

After dehydration of the in-house fabricated cantilever sample substrate on a hotplate at  $130\ ^\circ\text{C}$  for 10 min, the backside protective liner of the negative tone dry film photoresist (ADEX<sup>TM</sup>, DJ MicroLaminates) was removed and the resist was mechanically pressed to a corner of the bulk substrate but not the microcantilever beams themselves. We used either  $5\ \mu\text{m}$  or  $25\ \mu\text{m}$  thick dry film photoresists in this work. Roller lamination of the dry film photoresist was performed at  $65\ ^\circ\text{C}$ , at a speed of  $400\ \text{mm min}^{-1}$  (SKY-DSB 335R6 laminator) utilizing a  $1.0\ \text{mm}$  thick aluminum carrier plate followed by an additional annealing step at  $50\ ^\circ\text{C}$  for 5 min on a hotplate. In this manner, the dry resist films were reproducibly attached to the in-house fabricated microcantilevers. The topside protective liner was subsequently carefully removed prior to DFPL UV-exposure. The resist resolution is naturally

governed by the utilized exposure wavelength as well as the resist thickness. Thin  $5\ \mu\text{m}$  thickness negative tone dry film photoresists yield typically  $2\ \mu\text{m}$  resolution while thicker,  $25\ \mu\text{m}$  resist films can reach approximately  $5\ \mu\text{m}$  resolution. Soft contact UV-exposure using a Süss MJB3 mask aligner equipped with *i*-line filter (power density  $5.5\ \text{mW cm}^{-2}$ ) was done for 40 s and 80 s for  $5\ \mu\text{m}$  and  $25\ \mu\text{m}$  thick dry film photoresist, respectively. A post-exposure bake at  $85\ ^\circ\text{C}$  for 20 min was immediately performed successive to the UV-exposure. After cooling down the sample to room temperature, resist development was achieved in cyclohexanone within 3 min and 7 min for  $5\ \mu\text{m}$  and  $25\ \mu\text{m}$  thick resist films, respectively followed by an isopropanol rinse.

### 2.3. DFPL on commercial silicon nitride cantilevers by mask aligner or laser lithography

For the modification of commercial microcantilevers, silicon nitride AFM probes (PNP-DB, NanoWorld) with pyramidal tips of  $3.5\ \mu\text{m}$  height at the end of  $500\ \text{nm}$  thick microcantilevers were directly used as substrate material. These cantilevers come with a  $70\ \text{nm}$  thick reflective Cr/Au coating, which either before or after any etching modification was removed by immersing the sample in Lugol's solution for 10 s. The commercial cantilever probes were furthermore purchased as single pieces meaning they were not attached to a supporting structure anymore. In order to handle these probes and facilitate the application of the dry film photoresists, a plain adapter was manufactured. Here, a  $500\ \mu\text{m}$  thick (100)-Si wafer, which equals the AFM probe thickness, was diced at first to  $20 \times 20\ \text{mm}$  pieces. Successively, a rectangular slit of  $6.0\ \text{mm}$  by  $1.7\ \text{mm}$  was made by laser cutting to retain the AFM probe having a probe body size of  $3.4\ \text{mm}$  by  $1.6\ \text{mm}$ . This adapter together with the commercial cantilever as well as a carrier glass slide were all cleaned in NEP, acetone and isopropanol, followed by dehydration at  $130\ ^\circ\text{C}$  for 10 min on a hotplate. The adhesive Crystalbond 555 was applied immediately after the dehydration to fix the cantilever chip and adapter to the glass slide as shown in figure 2. Dry film photoresists of either  $5\ \mu\text{m}$  or  $25\ \mu\text{m}$  thickness were manually transferred and attached to the sample but omitting the aforementioned thermal roller laminator. Within this procedure, first the bottom protective liner was removed from the dry film photoresist and one corner of the film was firmly attached to the silicon adapter. The sample was then placed on a  $68\ ^\circ\text{C}$  hotplate causing thermal self-attachment of the dry film photoresist. A cotton swab was used to support homogeneous film adhesion but without putting too much pressure within the freestanding microcantilever region. After an additional annealing step of 5 min at  $50\ ^\circ\text{C}$  to further promote dry resist adhesion, the sample was placed on a stack of tissues and allowed to cool down to room temperature under ambient conditions. The remaining protective topside liner was subsequently gently removed. Reliable liner removal without partial dry film adhesion loss from the cantilever and tip was in some cases challenging, probably caused by the thickness difference between the silicon adapter and the cantilever probe. In this case the sample was repeatedly placed again on

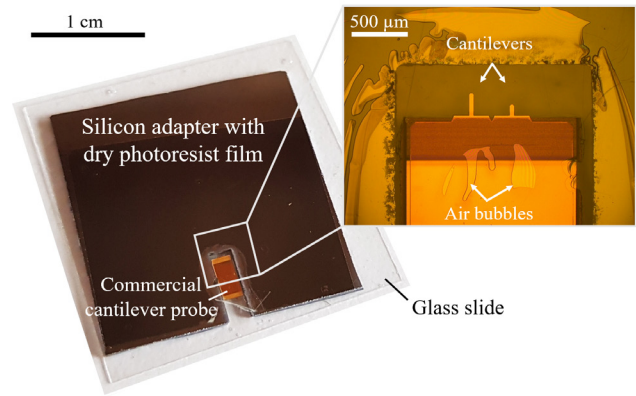


**Figure 2.** DFPL of commercial AFM cantilever probes requires an adapter to host the sample and to support dry film photoresist attachment. Shown on the left is the  $20 \times 20\ \text{mm}^2$  silicon adapter with the cantilever probe. Crystal bond was used as an adhesive to fixate the adapter and cantilever probe on a glass slide. The applied  $5\ \mu\text{m}$  dry film photoresist shown here adheres properly to the two microcantilever beams (right image) after removal of the upper liner. A complete elimination of air bubbles on the probe as indicated is difficult as hot roller lamination was not possible. Nevertheless, air bubbles were not observed on the cantilevers themselves.

the hotplate and annealed between  $55\ ^\circ\text{C}$  to  $65\ ^\circ\text{C}$  for a couple of seconds after removal of the protective topside liner until adequate adhesion was achieved. Exposure of the dry film photoresist was performed as described before in section 2.2.

Contact-free laser lithography of  $25\ \mu\text{m}$  dry film photoresists was also employed in conjunction with commercial cantilevers, using the same methods compared to the mask aligner exposure with respect to dry film photoresist adhesion, baking, and development. For laser lithography a  $\mu\text{PG}$  101 micropattern generator (Heidelberg Instruments) equipped with a  $375\ \text{nm}$  UV-laser source was used to expose and align the pre-assembled sample, using  $3.8\ \text{mW}$  laser power and  $5\ \text{mm}^2\ \text{min}^{-1}$  writing speed. The commercial probe contains four cantilevers, two at each opposing side. Opposing corners of the probe body as well as outer edges of each individual cantilever were manually chosen and served as alignment markers for the CAD-file exposure. The focus was manually set on the microcantilever beam. Laser lithography exposure was used to create a series of cylindrical pillars on commercial cantilevers, however those pillars were not used for the cell measurements and serve here only as a proof of concept of laser exposure of the dry film photoresists. In the following, unless otherwise stated, all fabricated structures on both in-house and commercial cantilever beams were fabricated using conventional mask aligner UV-exposure.

### 2.4. Post-modification procedures of freestanding microcantilever beams

**2.4.1. RIE of cantilevers.** Etching patterns into in-house fabricated and commercial silicon nitride cantilever beams was accomplished by  $\text{CF}_4$  plasma RIE for at least 15 min with settings already mentioned in section 2.1. The developed  $5\ \mu\text{m}$  thick dry film photoresist acts here as a stable etch mask. The

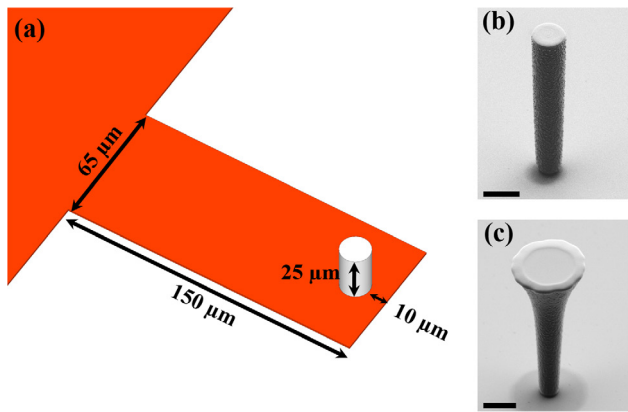


**Figure 3.** (a) Illustration of a dry film photoresist pillar on an in-house fabricated silicon nitride cantilever beam having a length of  $150\ \mu\text{m}$  and a width of  $65\ \mu\text{m}$ . The fabricated pillars were all  $25\ \mu\text{m}$  in height, with diameters varying from  $5\ \mu\text{m}$  to  $20\ \mu\text{m}$ . A distance of  $10\ \mu\text{m}$  was kept between the end of the cantilever and the outermost edge of the pillar. Figures (b) and (c) show hardbaked dry photoresist pillars using a photomask corresponding to a perspective  $5\ \mu\text{m}$  pillar diameter with and without utilized *i*-line filter during exposure, respectively. Scale bars  $5\ \mu\text{m}$ .

dry film photoresist was subsequently removed after RIE by immersing the samples in NEP at an elevated temperature of  $100\ ^\circ\text{C}$ . Any resist residues on the cantilevers at this point could be removed by an oxygen plasma treatment using the aforementioned settings in section 2.1.

**2.4.2. Metal deposition and lift-off on cantilever beams.** Metal patterns were created by the well-established lift-off procedure using  $5\ \mu\text{m}$  thick patterned dry film photoresists and physical vapor deposition of metals after resist development on in-house fabricated and commercial cantilevers. For metal deposition, a thermal electron-beam evaporator (Temescal FC-1800) was used to deposit first  $5\ \text{nm}$  titanium as an adhesion promotor followed by  $100\ \text{nm}$  aluminum. Lift-off was performed by immersing the sample in  $100\ ^\circ\text{C}$  NEP for approximately 1 h.

**2.4.3. Dry film photoresist as structural elements on cantilever beams.** In order to create single polymer pillars at the end of freestanding in-house fabricated microcantilevers,  $25\ \mu\text{m}$  thick dry film photoresists were used. Here, a circular area located  $10\ \mu\text{m}$  away from the freestanding end of the microcantilever beam (figure 3(a)) was exposed as described in section 2.2. One should be aware that the developed resist structures could potentially exhibit negative sidewalls, commonly referred to as so-called *T*-topping. This effect originates from strong absorption of UV-light below  $350\ \text{nm}$  in the resist surface [17], just as with the more common negative tone epoxy liquid photoresist SU-8. For this reason, we used an *i*-line filter to remove this part of the spectrum yielding sidewall angles much closer to  $90^\circ$  (figure 3(b)). Removal of the *i*-line filter triggers consequently the *T*-topping effect and enables a fabrication of pillars with negative sidewalls if desired (figure 3(c)). The resulting maximum diameter at the top of the pillar is more than doubled compared to the pillar shown in figure 3(b) that was exposed with an *i*-line filter.

Nevertheless, in this work only pillars with straight sidewalls were in particular studied and used for cell measurements. Following resist development, pillars of dry film photoresist remain standing upright and were subsequently hardbaked at  $175\ ^\circ\text{C}$  during 1.5 h and gradually cooled down to room temperature to increase their mechanical and chemical stability. Various pillar diameters such as  $5\ \mu\text{m}$ ,  $10\ \mu\text{m}$ ,  $15\ \mu\text{m}$  and  $20\ \mu\text{m}$  were fabricated in this manner. To assure full compatibility with conventional AFM operation, a  $5\ \text{nm}$  Ti adhesion layer and  $40\ \text{nm}$  Au layer were deposited by thermal evaporation on the cantilever backside as a reflective coating for laser-optical cantilever readout in the AFM.

AFM compatible cantilevers with resist pillars of  $15\ \mu\text{m}$  in diameter were exemplary chosen to perform cell elasticity measurements utilizing the JPK NanoWizard 4 on fixated NIH-3T3 mouse fibroblasts (ATCC) in standard phosphate buffered saline (PBS). The cells were grown overnight on fibronectin coated cover glasses, subsequently treated with 4% formaldehyde in PBS for 120 min and washed three times in PBS.

Data evaluation was done using the internal JPK data processing software which assumes the so-called Sneddon and Harding's contact model [18]. Following this model, for a flat-ended circular cylinder of radius  $a$ , here the dry film photoresist pillar radius, the loading part of force-distance curves are analysed to extract the elastic Young's modulus according to equation (1):

$$F = \frac{2E}{1 - \nu^2} \cdot a\delta \quad (1)$$

where  $F$  is the force,  $E$  is the Young's modulus,  $\nu$  is the Poisson ratio (set to 0.5), and  $\delta$  is the indentation depth.

The hardbaked dry film photoresist pillar has a Young's modulus of  $1\ \text{GPa}$  order of magnitude as stated by the manufacturer (DJ Microlaminates). The 3T3 mouse fibroblasts are expected to have an elastic modulus in the range of  $1\text{--}100\ \text{kPa}$  [19]. Since the elastic modulus of the dry resist pillars is orders of magnitude larger than the modulus of the cells, the Young's modulus,  $E$  in equation (1) should directly correspond to the Young's modulus of the cells. Equation (1) is the closest available approximation offered by the software for performing data analysis, and notably, disregards the cantilever probe inclination of  $12^\circ$  to the horizontal surface. Nevertheless, further work is required in future to fully validate and improve the model with respect to our large, flat-ended cylindrical pillars.

### 3. Results and discussion

Based on the aforementioned procedures, various etch patterns were realized for both in-house and commercial silicon nitride cantilevers. Etching of the cantilevers allows to alter their overall shape or to create certain 3D patterns on the cantilever beam itself. This is exemplary shown in figure 4, where holes of different diameter and arrangement were fully etched through the freestanding microcantilever beams. The depicted example was also chosen to show the

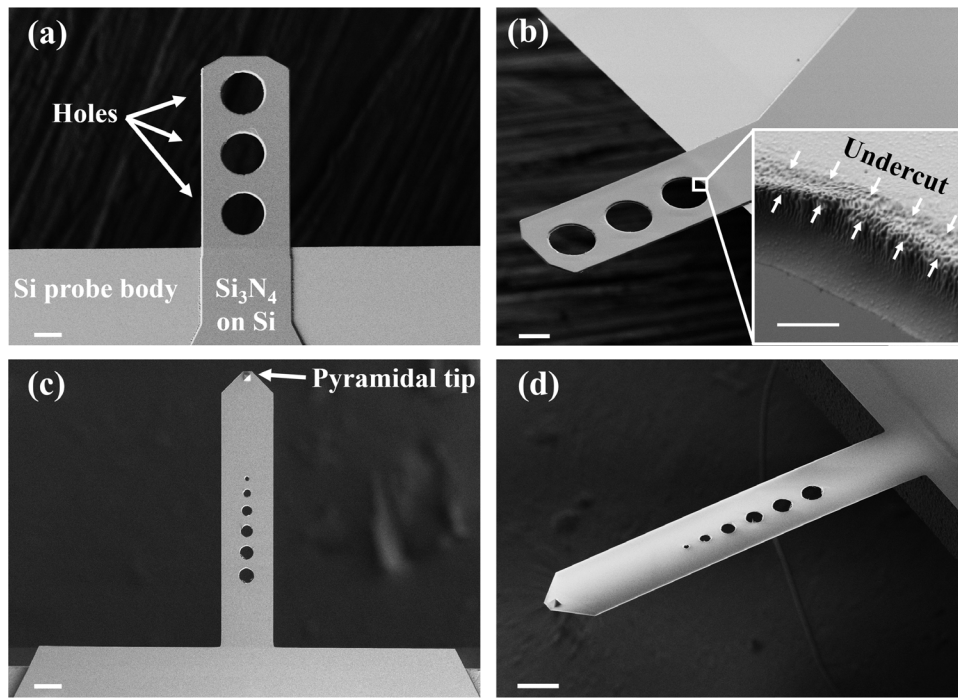


**Figure 4.** Circular holes etched through silicon nitride cantilevers by  $\text{CF}_4$  plasma RIE. (a) Displays a pattern of three  $30\ \mu\text{m}$  diameter holes etched through an in-house fabricated cantilever as viewed from above. Due to the manner of in-house cantilever fabrication by RIE of silicon nitride membranes the probe body displays silicon (Si) where silicon nitride has been etched. The corresponding side view (b) shows that the cantilever remains straight after etching and cleaning processes, and with the corresponding inset revealing the undercut as a step in the hole profile due to isotropic etch reactions. This undercut is approximately  $700\ \text{nm}$  when viewed from the top, however the length of the undercut was generally found to vary along the length of the beam and with the size of the holes. (c) and (d) Show the top- and side views of a commercial cantilever into which six holes of diameters between  $3\ \mu\text{m}$  and  $11\ \mu\text{m}$  were etched. Scale bars  $20\ \mu\text{m}$ , beside  $1\ \mu\text{m}$  scale bar of the inset in (b).

partly observed under-etching in the silicon nitride (figure 4(b)). Samples etched with  $\text{CF}_4$  plasma for 15 min exhibit a maximum undercut depth between  $0.2\ \mu\text{m}$  and  $0.9\ \mu\text{m}$ . The amount of under-etching increased with increased diameter of the circular hole, and with the distance away from the base of the cantilever. This effect is likely caused due to a certain adhesion loss of the dry resist at the extremities of the flexible cantilever beam. Etching methods with higher anisotropy, such as RIE with an inductively coupled plasma source [17], should significantly limiting under-etching. For our experiments, we found that an addition of 22 sccm Ar to the RIE process, while keeping all other etching parameters constant, decreased the intensity of the undercut by a factor of 2–3.

Custom etched structures could serve to accomplish complex MEMS structures and enable calorimetric spectroscopy [12], to tune cantilever resonance frequency [20] and to improve mass detection sensitivity [21, 22] to mention a few application scenarios. Notably, both in-house fabricated and commercial microcantilever beams kept their original angular alignment despite etching and cleaning, which enables still their full compatibility with the intended sensor and AFM applications. In order to etch through commercial cantilevers, as mentioned before, the backside reflective gold had to be removed. We found however that the AFM laser signal reflected from the etched commercial cantilevers was still sufficiently strong to perform AFM scans successfully. This may be explained by a few nanometers remnant

backside chromium, originally intended as adhesion layer for the thicker gold film. Redepositing a new reflective gold layer after commercial cantilever etching is therefore optional to insure AFM compatibility.

Advanced material patterning besides etching is furthermore an integral requirement for the assembly of electronic and sensing components, such as electrodes, on cantilever beams. For applications where photolithographic micropatterning suffices, DFPL offers as well a straightforward pathway to efficient large-scale material integration on microcantilever beams. As a general proof of concept, we show here the localized deposition of circularly shaped aluminum patterns (figure 5). Metal patterning was achieved, as mentioned before, by conventional wet lift-off in NEP. In principle, DFPL is not restricted in terms of the shape or size of the patterns as long they are in alignment with the resolution limit. It even enables metal deposition on cantilever beams that possess a pyramidal scanning tip. Although the process worked on both, in-house and commercial cantilevers, some commercial cantilevers showed signs of metal film adhesion failure despite the presence of a titanium adhesion promotor. Further investigations are still required to elucidate fully the reason of this issue. In this regard, the 3D morphology of the pyramidal tip must be discussed because adhesion loss was mainly observed near the tip base (supplementary figure S1 ([stacks.iop.org/JMM/29/025014/mmedia](https://stacks.iop.org/JMM/29/025014/mmedia))). Furthermore, commercial probe DFPL modification requires the aforementioned adapter,

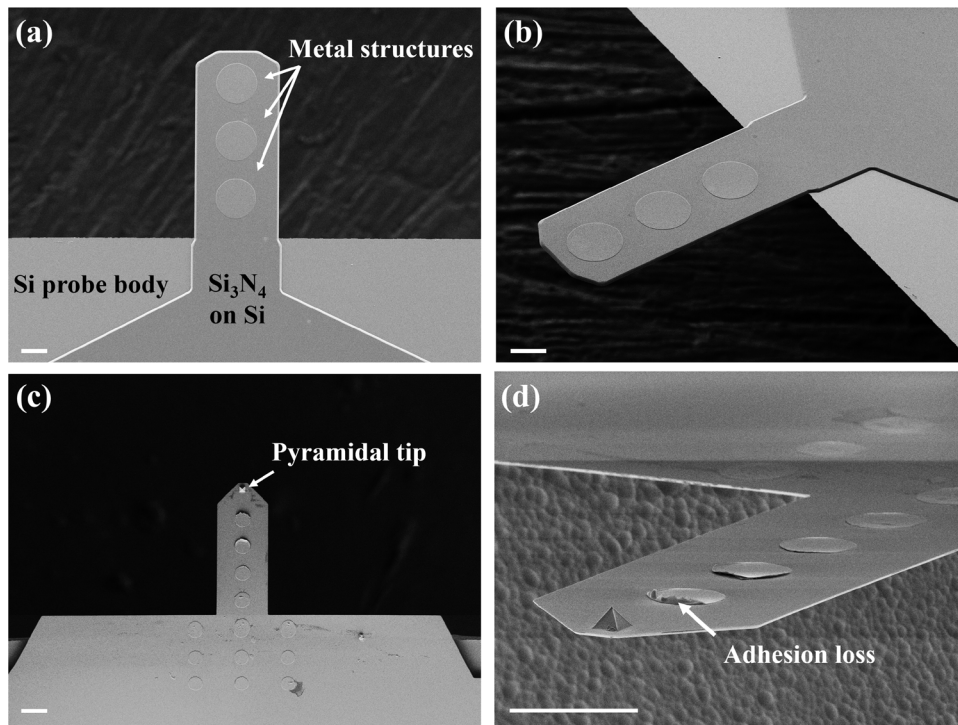


**Figure 5.** Creation of circular metal structures of 100 nm Al on silicon nitride cantilever beams: (a) top- and (b) side view of tipless in-house fabricated cantilever, and (c) top- and (d) side-view of commercial cantilever probes with a pyramidal scanning tip. The exaggerated side-view (d) reveals some adhesion issues on commercial cantilever probes closest to the tip. All scale bars 20  $\mu\text{m}$ .

which affects photoresist film adhesion in comparison to in-house fabricated cantilevers. Varying the adapter thickness by only 5–10  $\mu\text{m}$  had a significant impact on the success of DFPL modification. Here, adapters slightly thinner than the thickness of the cantilever probe body yielded better dry film photoresist adhesion and cantilever beam modification.

As discussed before, FIB milling, as demonstrated by Lavrik *et al* [12], and FIB material deposition represent alternatives to DFPL. FIB techniques understandably offer superior resolution in comparison to feature sizes of about 2  $\mu\text{m}$  that were achieved here with DFPL. However, as mentioned before, FIB techniques are rather expensive, time-consuming and hardly available when compared to the global availability of plain photolithography. Therefore, we believe that this DFPL technique can represent an inspiring and versatile basis for other researchers and small business manufacturers to develop or enhance existing microcantilever beam sensors, AFM probes and other flexible and 3D micropatterned components. Photolithography allows readily to be scaled-up to produce large quantities of a desired architecture. In addition, alignment markers can be readily implemented, e.g. during the microfabrication procedure of silicon nitride membranes to cantilevers, and assist subsequently the adjustment of further layers that shall be patterned by photolithography. A precise alignment of a photolithographic design on single commercial cantilevers is however more challenging using conventional mask aligners, as effective alignment markers are typically not present. Laser lithography enables however, alignment of the exposure pattern rather precisely based on certain cantilever features that serve as pseudo-alignment markers (cf. figure 8).

For a continued application of modified AFM probes with pyramidal scanning tips, the ability to perform AFM topography scans still after their modification is crucial. Here, a standard topography reference sample decorated with regular pits (VGRP-GS from Bruker Nano) was imaged by virgin PNP-DB AFM cantilevers, as well as by cantilever probes modified by either etching (figures 4(c) and (d)) or metal deposition (figures 5(c) and (d)). The scans were performed in contact mode (Bruker Bioscope Catalyst AFM) and the surface reconstructions by AFM (supplementary figure S2) lacked any observable differences that would serve otherwise as indication for a major tip geometry degradation.

After performing so-called zero order levelling on each topography image (NanoScope Analysis Software), the root-mean-square (RMS) roughness of the sample, excluding the scan regions associated with the etch pits ranged between 0.4 nm to 0.8 nm. This demonstrates that the implemented 5  $\mu\text{m}$  dry-photoresist films are capable to sufficiently protect the sharp 3.5  $\mu\text{m}$  high pyramidal tip during  $\text{CF}_4$  etching or metallization, and that DFPL impacts no significant influence on the AFM probe capabilities.

Besides its use as lithographic mask, dry-photoresist films can resemble functional elements themselves. Similar to the well-established negative tone epoxy resist SU-8, dry film photoresists can be used as a permanent protective layer, e.g. to encapsulate electrical contacts or as shown here, directly as a scanning tip or indenter. Based on 25  $\mu\text{m}$  thick dry film photoresists, single circular areas, yielding after hardbake a flat-ended cylindrical pillar at the end of the freestanding microcantilever beam, were fabricated. Flat-ended cylindrical pillars with an aspect ratio as high as 1:5 were achievable

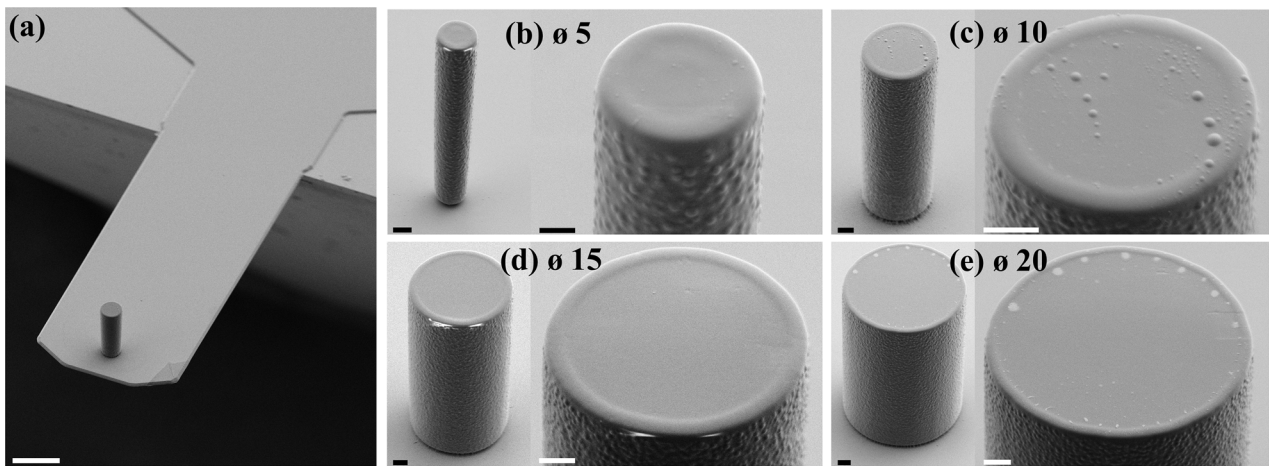


**Figure 6.** Hardbaked dry photoresist pillars of 25  $\mu\text{m}$  height on in-house fabricated silicon nitride cantilevers. (a) Shows the entire cantilever with a pillar of 15  $\mu\text{m}$  diameter (scale bar 20  $\mu\text{m}$ ). Various pillars are shown in two different magnification with (b) 5  $\mu\text{m}$ , (c) 10  $\mu\text{m}$ , (d) 15  $\mu\text{m}$ , and (e) 20  $\mu\text{m}$  diameter. All scale bars (b)–(e) are 2  $\mu\text{m}$ . Bumps of approximately 0.4  $\mu\text{m}$  diameter are present at the sidewalls of all pillars regardless of their size, as well as an elevated outer rim around the top surface. The bright spots present around the upper surface of the pillars in (d) and (e) originate from charging effects during scanning electron microscopy.

using 25  $\mu\text{m}$  thick resist films. In principle, pillar diameters of some hundreds of nanometers smaller than 5  $\mu\text{m}$  are also realizable with 25  $\mu\text{m}$  dry film photoresist thickness, however they showed frequently a tendency for complete or partial bending. In order to further shrink down the pillar diameters while keeping a vertical pillar alignment, 5  $\mu\text{m}$  thick dry film photoresists were used and enabled diameters down to 1.8  $\mu\text{m}$ . In this regards, we emphasize again the need for an *i*-line filter during the UV-exposure of the dry resist to avoid the *T*-topping effect that would otherwise prevent straight sidewalls formation (see figure 3(c)).

Pillars of 25  $\mu\text{m}$  in height having diameters of 5  $\mu\text{m}$ , 10  $\mu\text{m}$ , 15  $\mu\text{m}$  and 20  $\mu\text{m}$  are shown in figure 6. The results show consistently an elevated outer rim on the top surface of the pillar with a width between 0.6  $\mu\text{m}$  to 0.8  $\mu\text{m}$ . Beside the rim, the top surface can be mainly considered flat. Although here of only minor importance, we also show one example of a 10  $\mu\text{m}$  diameter dry resist pillar (figure 6(c)), which exhibits some bumps of sizes ranging between less than 0.1  $\mu\text{m}$  to 0.4  $\mu\text{m}$  diameter. The origin of these partly observed bumps is still unknown. However, we speculate that they either originate from inherent features of the dry film photoresist or that they form during dry resist film processing. The dry resist pillar sidewalls exhibit consistently a rough surface structure again of bumps between 0.3  $\mu\text{m}$  to 0.4  $\mu\text{m}$  diameter, which was observed also prior to hardbake. For cell indentation with the resist pillars as discussed shortly, the roughness of the pillar sidewalls will likely not pose an issue, as the effective contact area should be hardly affected by such small bumps.

To evaluate the AFM topography-imaging quality of the resist pillars, a reference sample of silicon nitride with square pits of 26.3  $\times$  26.1  $\mu\text{m}$  in dimension, and 235 nm depth was fabricated. The sample was imaged in contact mode using an 11  $\mu\text{m}$  diameter dry resist pillar. The obtained images were compared to those acquired of the same sample but using a cantilever with a sharp 3D scanning tip (Otespaw, Veeco). Lateral tip-broadening effects were observed for the pillar

tip, as expected, since a larger scanning tip does not allow accurate tracing of fine sample features. The vertical measurements relating to pit depth were however in complete agreement between the two scanning probe tips. With the dry resist pillar, the slope of the pit sidewalls increased by a factor of 7–8 compared to the Otespaw probe and therefore, a decrease in lateral pit width of 25% was observed along the scan axis when measured along the pit bottom (supplementary figure S3). Our observations are in agreement with simple geometric considerations of a contact mode scan, where pillar and cantilever are assumed to be rigid, and the pit sidewalls are assumed to be completely vertical. Notably, no detrimental plastic deformation could be observed by scanning electron microscopy inspection of the pillar and cantilever after several hours of AFM imaging.

As discussed before, the flat-ended pillars were particularly designed for cell measurements. In comparison to probes equipped with a conventional sharp pyramidal tip or with a spherical indenter, flat-ended cylindrical AFM probes provide some advantages. Notably, the contact area of pyramidal tips will change significantly during indentation, which is also true but assumed to be more defined for spherical tip geometries [23]. In comparison to these tips, flat-ended cylindrical pillars offer roughly a constant contact area in a wider indentation range. This is especially important for adhesion measurements that highly depend on the contact area between the probing tip and sample surface [23–26] and for soft samples, such as living cells, that would otherwise suffer from high local, and potentially even destructive strains [23, 27]. These benefits however are here intimately linked to a reduced lateral resolution based on the larger tip radius in comparison to sharp pyramidal AFM tips. On the other hand, cells can in principle be considered as inhomogeneous entities that consist of several components, which lead to a significant spatial variation of elastic properties over the cell body [28]. Flat-ended probes with larger surface area compared to sharp pyramidal tips should consequently excel here in comparison at measuring

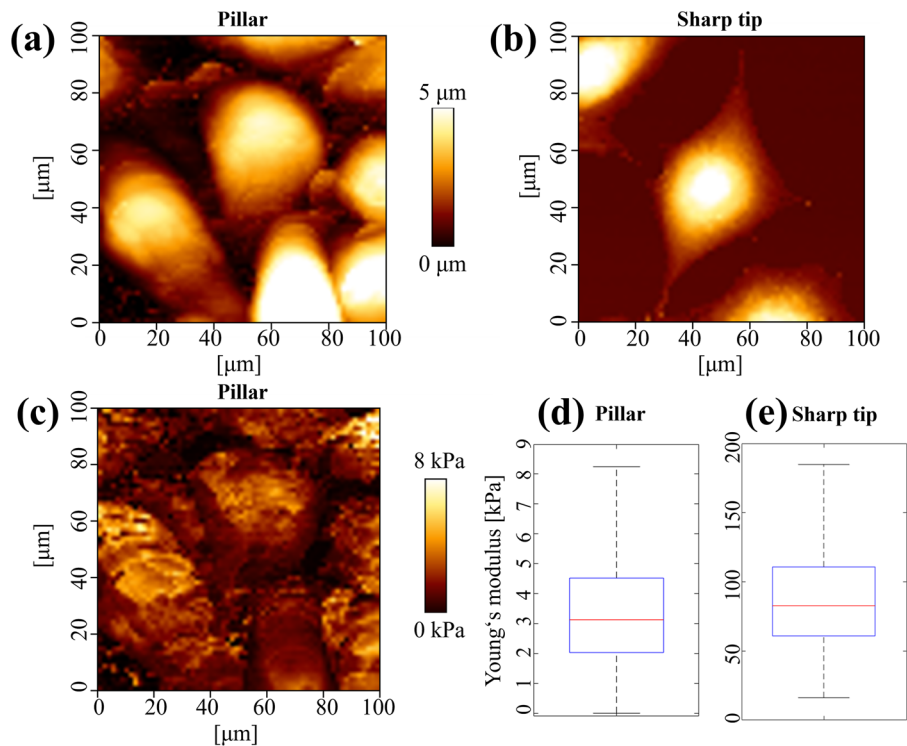


**Figure 7.** (a) Topography image of fixated 3T3 mouse fibroblasts imaged using a  $25\ \mu\text{m}$  high,  $15\ \mu\text{m}$  diameter hardbaked dry photoresist pillar on an in-house fabricated silicon nitride cantilever. The image indicates significant tip broadening of the cells due to the large pillar diameter as compared to (b), where imaging was performed with a sharp pyramidal tip, consequently rendering a more accurate image of the size and shape of a typical 3T3 mouse fibroblast. Notice that the scan areas as well as the cell densities in (a) and (b) are different. In (c) the Young's modulus image corresponding to the topography image (a) using the  $15\ \mu\text{m}$  diameter resist pillar is shown. It indicates a homogeneous distribution of elastic moduli over the entire sample. The cell nuclei show slightly higher values, while the space between cells appear slightly softer. The corresponding median and variation of the elastic modulus are represented by boxplots in (d) for the dry resist pillar, and (e) for the sharp tip. Median values of 3.1 kPa and 82.7 kPa were found respectively.

the entire cell's response or mechanical properties of tissue rather than a local state [23, 28]. The impact of the tip geometry onto the measured cell elastic properties is extensively discussed elsewhere [23, 26, 29, 30]. Here, it was observed that pyramidal tips generally tend to yield for instance a larger elastic modulus caused by the strong local curvature of the pyramidal tip apex compared to flat-ended or spherical tips, however the topic is still debated. The determination of cell adhesion as well as elastic properties implementing cylindrical flat-ended silicon AFM probes was also shown previously [24, 25]. Those tips were self-fabricated based on FIB milling of commercial AFM probes. Flat-ended tips fabricated by FIB milling are also commercially available (Nanosensors PL2-series) and retail at roughly 2 to 3 times the price of conventional tapping-mode silicon cantilevers (here comparing with Nanosensors PPP-CONT and PL2-CONTR cantilevers). Using dry film photoresists to make such flat-ended pillars would substantially reduce costs. As a proof of concept for the usability of these polymeric pillars, our in-house fabricated scanning probes with hardbaked dry photoresist pillars were exemplary used to image and measure mechanical properties of 3T3 mouse fibroblast cell cultures. Typical fibroblasts are  $30\ \mu\text{m}$  in diameter and  $5\ \mu\text{m}$  in height. We chose therefore the larger  $15\ \mu\text{m}$  diameter for a first demonstration of dry resist pillars to perform mechanical measurements. The  $15\ \mu\text{m}$  pillars provide a larger contact surface to the sample compared

to the smaller  $5\ \mu\text{m}$  pillars, despite a loss of lateral imaging resolution. While the measured mechanical cell response should originate from the entire cell, a lower lateral resolution was observed as expected (figure 7(a)). Imaging the cells with a sharp pyramidal tip having a tip radius below 10 nm (MSNL, Bruker Nano) naturally provides higher image resolution (figure 7(b)). Nevertheless, the measured cell heights of  $5\ \mu\text{m}$  are consistent for both cases. The corresponding Young's modulus determined with the large diameter cylindrical pillars displays an approximately homogenous value with a median of 3.1 kPa over the scanned cell area (figures 7(c) and (d)). In comparison to measurements performed with the sharp pyramidal tip, where values of around 82.7 kPa were determined (figure 7(e)). This value is of the same order of magnitude as shown by Codan *et al* [19] and demonstrates furthermore experimentally again the expected major influence of the tip geometry on the cell's mechanical properties. The variation in measured Young's modulus with the sharp tip (figure 7(e)) is also more than an order of magnitude higher than what was found with the dry resist pillar (figure 7(d)). Intuitively we can understand this greater variation in Young's modulus based on the high lateral localization of the sharp tip with the cells. Not only does the sharp tip measure the cells' mechanical response at a smaller area, it is also capable of punching into and through the cells, which suggests the substrate onto which the cells are grown have a noticeable

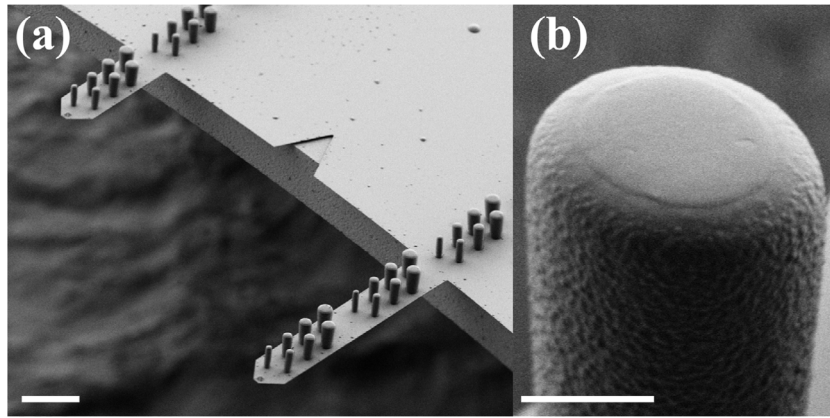


**Figure 8.** (a) Ensembles of dry photoresist pillars of diameters ranging from  $5\ \mu\text{m}$  to  $11\ \mu\text{m}$  were made on commercial AFM cantilever probes by means of laser lithography. Straight resist pillars with diameters as small as  $5\ \mu\text{m}$  could be created. Scale bar  $50\ \mu\text{m}$ . (b) Magnified area showing the top surface structure of an  $11\ \mu\text{m}$  diameter pillar. Scale bar  $5\ \mu\text{m}$ .

effect on the measured mechanical properties. The cylindrical pillar is in contrary able to average the mechanical response from a larger cell area, thus yielding a smaller variation in the measured Young's modulus. In conclusion, our results indicate that cylindrical flat-ended tips on AFM cantilever probes are usable for AFM measurements and appear beneficial for averaging the Young's modulus within a certain area. Hence, these probes can be capable tools for the determination of the average mechanical properties of cell ensembles. Nevertheless, an enhanced understanding of the mechanics, working principles and geometry effects of the cylindrical dry resist pillars for cell elasticity measurements are still required and subject to further research.

Finally, we show results of DFPL using a laser lithography device. Laser lithography is a contactless and therefore non-destructive patterning strategy, whereas utilization of a mask aligner with a sample brought in contact with a photomask might potentially be harmful particular for fragile samples. Laser assisted lithography is also more versatile than conventional mask aligner photolithography since device designs can be readily implemented without the need of a physical photomask. This allows quick implementation of new designs and individual manufacturing. Shown in figure 8 are hardbaked  $25\ \mu\text{m}$  tall dry photoresist pillars of various diameters fabricated by laser lithography on commercial silicon nitride cantilevers. Employing laser exposure produces pillar sidewalls close to  $90^\circ$  that notably exhibit again bumps at their sidewall, which appears to be an inherent feature of the dry film photoresist. In comparison to conventional photolithography, as discussed before, pillars of  $5\ \mu\text{m}$  in diameter represent again the smallest mechanically stable structure. A key benefit of laser lithography is that individual pattern alignment and exposure can be realized with ease for individual cantilever beams and even structural elements, which provide further degrees of freedom in device design. The top surface profiles of laser-exposed dry resist pillars as shown in figure 8 differ however if compared to the aforementioned mask aligner lithography (see figure 6). Pillars fabricated by laser lithography do not display the effect of an elevated outer rim (figure 8(b)). Additional exposure tests on planar silicon

nitride substrates with enabled pneumatic autofocus system, which automatically focuses the laser onto the resist surface, yielded again pillars similar to those fabricated by the mask aligner. This indicates that the altered surface profile of the dry resist pillars observed on the commercial cantilevers is an effect of a manual focus setting of the laser beam, which is naturally located at the cantilever surface,  $25\ \mu\text{m}$  below the top surface of the dry film photoresist.

#### 4. Conclusion

We have demonstrated DFPL directly on freestanding AFM compatible silicon nitride microcantilevers. Compared to competing methods, benefits are provided by the fact that only plain optical lithography systems and a thermal laminator are required, which is furthermore linked to a potential reduction in cost and time. DFPL avoids in particular the commonly encountered issue of resist edge-beads and inhomogeneous resist coverage during liquid resist spin-coating on freestanding 3D microstructures.

On both, commercial cantilevers with a pyramidal tip and in-house fabricated tipless cantilevers, custom patterns were directly created by either  $\text{CF}_4$  based RIE or localized metal deposition. Comparative AFM topography scans using our DFPL customized and virgin commercial AFM cantilevers gave similar results. In terms of resolution,  $5\ \mu\text{m}$  thick dry film photoresists allowed in our experiments to pattern microstructures with  $2\ \mu\text{m}$  feature size. Additionally, stable flat-ended cylindrical dry photoresist pillars up to  $25\ \mu\text{m}$  in height were fabricated at the freestanding end of microcantilever beams. The resist pillar structures showed partly a mechanical instability for aspect ratios higher than 1:5 using  $25\ \mu\text{m}$  thick dry film photoresists. We showed furthermore that polymer pillar probes can be employed for elasticity measurements of 3T3 mouse fibroblast cell cultures. The demonstrated DFPL protocol can be readily adaptable to various end-user scenarios and provides a rapid and facile microfabrication strategy for freestanding microcantilever beams and other microsystems.

## Acknowledgments

The financial support by the Ministry of Education and Research Germany (BMBF: NanoMatFutur: 13N12545) as well as by the German Research Foundation (DFG: Research Training Group GRK 2203) is gratefully acknowledged. Furthermore, we thank S Jenisch, C Weich and A Minkow at Ulm University for their experimental support and technical assistance.

## ORCID iDs

Madeleine Nilsen  <https://orcid.org/0000-0003-3035-4718>

## References

- [1] Lang H P, Hegner M and Gerber C 2010 *Springer Handbook of Nanotechnology* ed B Bhushan (Berlin: Springer) pp 427–52
- [2] Gaitas A and French P 2012 Piezo-thermal probe array for high throughput applications *Sensors Actuators A* **186** 125–9
- [3] Wang J, Feng B, Wu W and Huang Y 2011 Chemisorption sensing and analysis using silicon cantilever sensor based on *n*-type metal-oxide-semiconductor transistor *Microelectron. Eng.* **88** 1019–23
- [4] Toffoli V, Carrato S, Lee D, Jeon S and Lazzarino M 2013 Heater-integrated cantilevers for nano-samples thermogravimetric analysis *Sensors* **13** 16657
- [5] Hofer M, Ivanov T, Rudek M, Kopiec D, Guliyev E, Gotszalk T P and Rangelow I W 2015 Fabrication of self-actuated piezoresistive thermal probes *Microelectron. Eng.* **145** 32–7
- [6] Xu P, Li X, Yu H and Xu T 2014 Advanced nanoporous materials for micro-gravimetric sensing to trace-level bio/chemical molecules *Sensors* **14** 19023
- [7] Xu J, Bertke M, Li X, Mu H, Zhou H, Yu F, Hamdana G, Schmidt A, Bremers H and Peiner E 2018 Fabrication of ZnO nanorods and Chitosan@ZnO nanorods on MEMS piezoresistive self-actuating silicon microcantilever for humidity sensing *Sensors Actuators B* **273** 276–87
- [8] Schlur L, Hofer M, Ahmad A, Bonnot K, Holz M and Spitzer D 2018 Cu(OH)<sub>2</sub> and CuO nanorod synthesis on piezoresistive cantilevers for the selective detection of nitrogen dioxide *Sensors* **18** 1108
- [9] Wasisto H S, Merzsch S, Waag A, Uhde E, Salthammer T and Peiner E 2013 Airborne engineered nanoparticle mass sensor based on a silicon resonant cantilever *Sensors Actuators B* **180** 77–89
- [10] Sečianska K, Šoltýs J and Cambel V 2017 Study of magnetic micro-ellipses by cantilever sensor *Acta Phys. Pol. A* **131** 833–5
- [11] Dobroth T and Erwin L 1986 Causes of edge beads in cast films *Polym. Eng. Sci.* **26** 462–7
- [12] Lavrik N V, Sepaniak M J and Datskos P G 2004 Cantilever transducers as a platform for chemical and biological sensors *Rev. Sci. Instrum.* **75** 2229–53
- [13] Han A, Kuan A, Golovchenko J and Branton D 2012 Nanopatterning on nonplanar and fragile substrates with ice resists *Nano Lett.* **12** 1018–21
- [14] Yun J, Kang G, Park Y, Kim H W, Cha J-J and Lee J-H 2016 Electrochemical impedance spectroscopy with interdigitated electrodes at the end of hypodermic needle for depth profiling of biotissues *Sensors Actuators B* **237** 984–91
- [15] Zhang J, Con C and Cui B 2014 Electron beam lithography on irregular surfaces using an evaporated resist *ACS Nano* **8** 3483–9
- [16] Chang J, Zhou Q and Zettl A 2014 Facile electron-beam lithography technique for irregular and fragile substrates *Appl. Phys. Lett.* **105** 173109
- [17] Madou M J 2011 *Manufacturing Techniques for Microfabrication and Nanotechnology* (Boca Raton, FL: Taylor and Francis)
- [18] Harding J W and Sneddon I N 1945 The elastic stresses produced by the indentation of the plane surface of a semi-infinite elastic solid by a rigid punch *Math. Proc. Camb. Phil. Soc.* **41** 16–26
- [19] Codan B, Martinelli V, Mestroni L and Sbaizero O 2013 Atomic force microscopy of 3T3 and SW-13 cell lines: an investigation of cell elasticity changes due to fixation *Mater. Sci. Eng. C* **33** 3303–8
- [20] Rinaldi G, Packirisamy M and Stiharu I 2008 Frequency tuning AFM optical levers using a slot *Microsyst. Technol.* **14** 361–9
- [21] Lavrik N V and Datskos P G 2003 Femtogram mass detection using photothermally actuated nanomechanical resonators *Appl. Phys. Lett.* **82** 2697–9
- [22] Dong F W, Xu D, Xin W, Tsuyoshi I and Ryutaro M 2016 Improving picogram mass sensitivity via frequency doubling in coupled silicon micro-cantilevers *J. Micromech. Microeng.* **26** 015006
- [23] Chen J 2014 Nanobiomechanics of living cells: a review *Interface Focus* **4** 20130055
- [24] Rico F, Roca-Cusachs P, Sunyer R, Farre R and Navajas D 2007 Cell dynamic adhesion and elastic properties probed with cylindrical atomic force microscopy cantilever tips *J. Mol. Recognit.* **20** 459–66
- [25] Acerbi I, Luque T, Giménez A, Puig M, Reguart N, Farré R, Navajas D and Alcaraz J 2012 Integrin-specific mechanoresponses to compression and extension probed by cylindrical flat-ended AFM tips in lung cells *PLoS One* **7** e32261
- [26] Gavara N 2017 A beginner's guide to atomic force microscopy probing for cell mechanics *Microsc. Res. Tech.* **80** 75–84
- [27] Lekka M 2016 Discrimination between normal and cancerous cells using AFM *BioNanoScience* **6** 65–80
- [28] Haase K and Pelling A E 2015 Investigating cell mechanics with atomic force microscopy *J. R. Soc. Interface* **12** 20140970
- [29] Vargas-Pinto R, Gong H, Vahabikashi A and Johnson M 2013 The effect of the endothelial cell cortex on atomic force microscopy measurements *Biophys. J.* **105** 300–9
- [30] Chiou Y-W, Lin H-K, Tang M-J, Lin H-H and Yeh M-L 2013 The influence of physical and physiological cues on atomic force microscopy-based cell stiffness assessment *PLoS One* **8** e77384